ACS OMEGA

Open Access

http://pubs.acs.org/journal/acsodf

Article

Lanthanum-Integrated Porous Adsorbent for Effective Phosphorus Removal

Yalin He, Xingyue Qi, Jialong Li, Wendi Wang, Jingyu Zhang, Lanhao Yang, Mei Xue,* and Kun Lan*

Cite This: *ACS Omega* 2024, 9, 30826−30833

Read Online

ACCESS | Metrics & More | Article Recommendations | Supporting Information

ABSTRACT: In pursuit of accessing clean water, the phosphate removal is of great importance for preventing eutrophication toward sustainable ecology. However, effective adsorbents with high capacity, selectivity, and long-term stability for treating phosphate in water still remain desired, which requires further development. Herein, a type of porous La-based adsorbents, which are composed of highly dispersed $La(OH)_3$ on amino-functionalized Caragana korshinskii (CK) nanowires, are designed and fabricated through simple amination and decoration of lemon bars. Specifically, the adsorption to phosphate can be quickly completed within 50 min, and an ultrahigh adsorption capacity of 173.3 mg of P g^{-1} is realized. Moreover, these composite adsorbents display excellent selectivity and anti-interference ability to phosphate in the presence of common anions (CO_3^{2-}, NO^{3-}, Cl^-, and SO_4^{2-}). After four regenerations, there is still a removal rate of 85%. This study underscores an integrated material model for designing advanced structures toward efficient wastewater treatment.

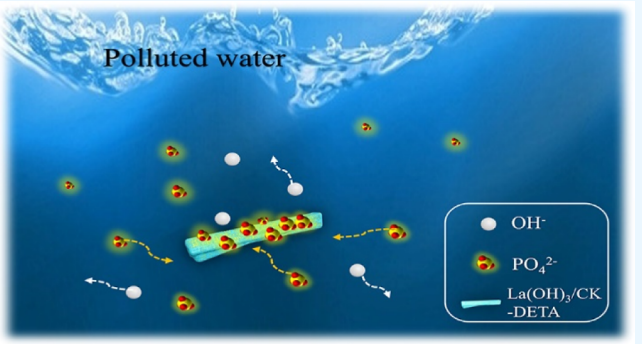

1. INTRODUCTION

As a pursuit of sustainable ecology and human health, access to clean water has readily been receiving great research attention. With the rapid development of industrialization, the growing amounts of unsustainable pollutants containing total organic carbon (TOC), heavy metals, and toxic ions have caused considerable environmental issues.[1−4] For instance, toxic heavy metals have led to serious biosafety issues due to bioaccumulation and persistence.[5] Excessive organic pollutants in water can produce hazardous reducing gases derived from anaerobic reactions, severely destructing ecosystems in water for organism survival.[6,7] Pollution treatment in water is of great importance,[8] and various strategies have been devoted to addressing environmental pollution problems over the past decades, including sedimentation, coagulation, and liquid extraction.[9] These methods do not eliminate the contaminants and allow for only simple treatment. Other methods, such as biological methods, ion exchange, and reverse osmosis,[10] generally cause toxic secondary pollution to the environment. Each approach for water treatment has advantages and drawbacks, which still needs to be further developed.

Among numerous pollutants, the removal of phosphates in water is one of the crucial issues for ecological sustainability since phosphorus is an essential nutrient element for plants,[11,12] but excessive phosphorus nutrients lead to eutrophic water bodies and algal blooms.[13,14] So far, various treatment technologies have been developed for removing or recovering phosphate from contaminated waters.[15−18] Adsorption is reckoned as a promising pathway for wastewater treatment because aqueous phosphorus can be both physically and chemically accumulated to the surface of adsorbents with advantageous simple operation, low cost, and high efficiency.[19] A variety of adsorbents such as metal oxides/hydroxides, metal−organic frameworks, zeolites, porous silicon, and biopolymers[20−29] have been employed. Lanthanum (La)-based compounds have emerged in various adsorbents due to their strong affinity to phosphates, but the low efficiency is a limitation, caused by aggregation in water.[11,30,31] The phosphate adsorption capacity can be largely promoted through nanostructuring La compounds into high-surface-area adsorbents, which possess improved dispersivity and exposed active sites.[32−40] Although some achievements have been made in phosphorus removal, most of the reported La-based adsorbents have drawbacks such as high cost and unsatisfactory adsorption capacity and stability,[19,41,42] which hinder their practical applications. Therefore, the rational design and scale-up synthesis of high-performance adsorbents with desirable cyclability for phosphate removal from water bodies remains a huge challenge.

Received: April 11, 2024
Revised: June 12, 2024
Accepted: June 18, 2024
Published: July 2, 2024

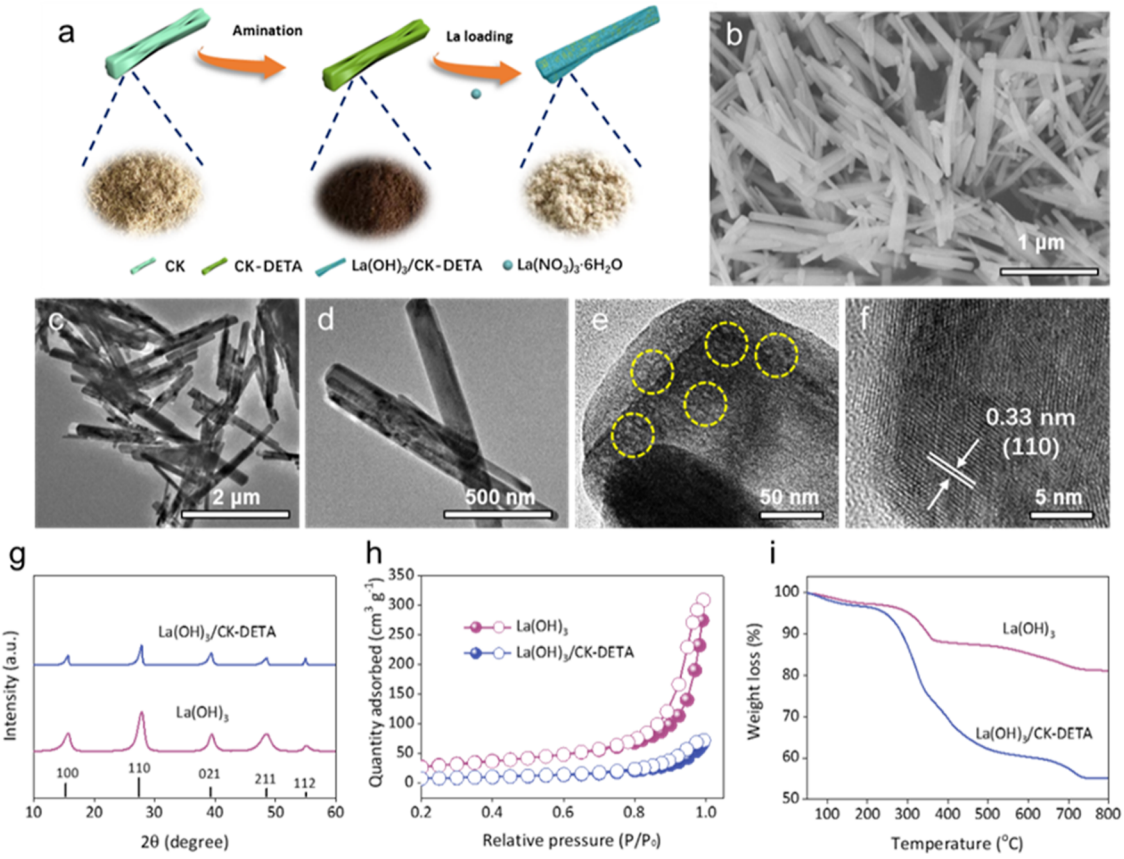

Figure 1. Material characterizations of the $La(OH)_3$/CK-DETA composite. (a) Synthetic process of the $La(OH)_3$/CK-DETA composite. (b) FESEM image and (c−e) TEM images with different magnifications of the $La(OH)_3$/CK-DETA composite. (f) HRTEM image recoded on the individual $La(OH)_3$/CK-DETA nanorods. (g) WAXRD patterns, (h) nitrogen sorption isotherms, and (i) TGA curves of pure $La(OH)_3$ and the $La(OH)_3$/CK-DETA composite.

In this work, a porous La-based adsorbent [$La(OH)_3$/CK-DETA] was prepared by a simple in situ growth method. The composite adsorbent was prepared by first simple amination of CK nanowires with diethylenetriamine (DETA) and then in situ decoration of lanthanum nitrate hexahydrate. The prepared composite adsorbent has highly dispersed $La(OH)_3$ on the CK surface due to the bonding of amines, which solves the problem of the severe agglomeration and difficult dispersion of $La(OH)_3$. Meanwhile, the high specific surface area of 45 m^2/g and the large mesopore size of 29.8 nm of the adsorbent were favorable for the adsorption of phosphate. This design not only provides a highly exposed porous structure for phosphate access and rapid mass transfer but also integrates physisorption and chemisorption into one composite material, resulting in an ultrahigh phosphate adsorption capacity and good cycling stability. As expected, the $La(OH)_3$/CK-DETA adsorbent exhibits an ultrahigh adsorption capacity of 173.3 mg P g^{-1} in a chemisorption behavior of a single molecular layer, surpassing most of the currently reported phosphate adsorbents. Meanwhile, the adsorption equilibrium can be reached within 50 min, demonstrating a very fast adsorption rate to phosphate. Such a composite adsorbent further shows excellent selectivity to phosphate against Cl^-, NO_3^-, CO_3^{2-}, and SO_4^{2-} and good reproducibility (85% retention over 4 cycles) to phosphate in simulated pollution treatment.

2. MATERIALS AND METHODS

2.1. Materials. The Caragana korshinskii (CK) was purchased from Inner Mongolia Co. Ltd. China. Lanthanum nitrate hexahydrate [$La(NO_3)_3·6H_2O$], DETA, formaldehyde (HCHO), hydrochloric acid (HCl), sodium phosphate monobasic (NaH_2PO_4), and sodium hydroxide (NaOH) were all purchased from Sinopharm Chemical Reagent Co. Ltd. China. All of the chemicals were directly used without further purification.

2.2. Preparation of $La(OH)_3$/CK-DETA. The La-based porous adsorbent was synthesized through a facile amino-functionalization and postdecoration process, as depicted in Figure 1a. Typically, after crushing the original CK through a 140-mesh sieve, 5.0 g of CK was immersed into 100 mL of NaOH solution (0.1 M). Then, 16.0 mL of DETA and 16.0 mL of HCHO were added slowly. The mixed solution was transferred to a thermostatic water bath stirred at 60 °C for 5 h. The mixture was cooled down to room temperature, and the pH of the solution was adjusted to 2−3. The functionalized CK-DETA was collected after centrifugation, washed several times, and dried in an oven. Afterward, 2.0 g of the obtained CK-DETA was added into 30 mL of deionized water, followed by the addition of 4.0 g of $La(NO_3)_3·6H_2O$. After that, the pH of the solution was adjusted to 10 before the mixture was stirred at 60 °C for 2 h and then at room temperature for another 24 h. The final product $La(OH)_3$/CK-DETA was obtained after centrifugation, washing, and drying in an oven.

https://doi.org/10.1021/acsomega.4c03501
ACS Omega 2024, 9, 30826−30833

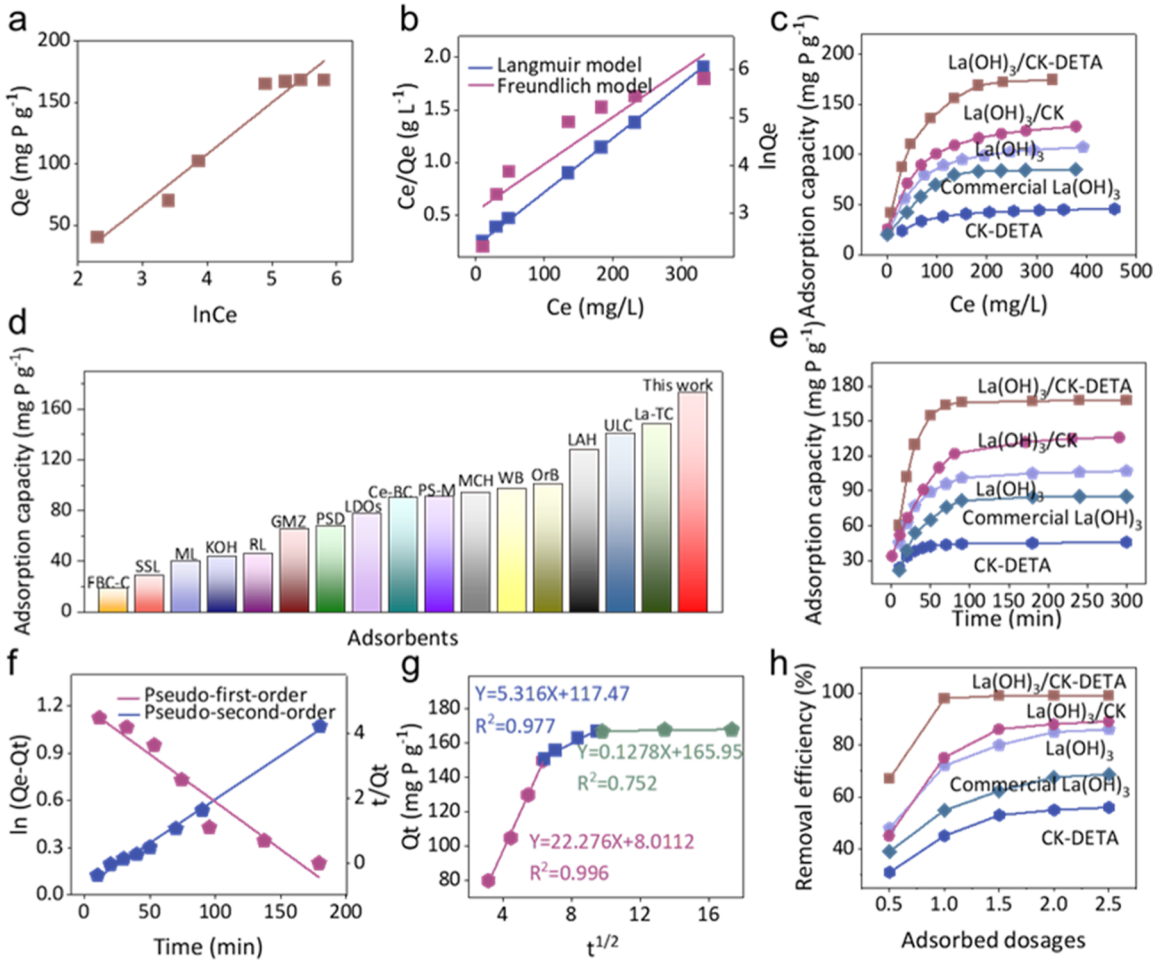

Figure 2. (a) Temkin and (b) Langmuir and Freundlich adsorption isotherm models of the $La(OH)_3$/CK-DETA adsorbent. (c) Phosphate adsorption capacity of CK-DETA, $La(OH)_3$, commercial $La(OH)_3$, $La(OH)_3$/CK, and $La(OH)_3$/CK-DETA adsorbents. (d) Summarized adsorption capacities of the reported adsorbents. (e) Adsorption rates of the CK-DETA, $La(OH)_3$, commercial $La(OH)_3$, $La(OH)_3$/CK, and $La(OH)_3$/CK-DETA adsorbents. (f) Pseudo-first-order and pseudo-second-order and (g) intraparticle diffusion models of $La(OH)_3$/CK-DETA. (h) Relationship between adsorbed dosage and removal efficiency of the five adsorbents.

2.3. Adsorption Experiments. To comprehensively evaluate the adsorption performance of the adsorbent for phosphate, a series of adsorption experiments were carried out. First, a certain amount of Na_2HPO_4 was dissolved into deionized water to prepare a phosphate solution with a concentration of 500 mg P L^{-1} as the raw solution of simulated wastewater. Then, 0.1 g of the adsorbent was added to 0.1 L of diluted phosphate solution (100 mg of P L^{-1}). The resulting mixture was shaken for 5 h at room temperature at a constant speed of 40 rpm. Lastly, a 0.45 μm aperture filter membrane was used to filter the mixture, and the concentration of phosphate was measured by a UV−vis spectrometer. The adsorption capacity of the adsorbent for phosphate (q_e) is calculated as follows.

$$q_e = (C_0 - C_e)V/m$$

where C_0 and C_e are the concentrations of phosphate in the initial and equilibrium solutions, respectively. V represents the solution volume and m is the adsorbent weight. For adsorption isotherms, 0.1 g of the adsorbent was added to a series of polyethylene tubes containing 0.1 L of phosphorus solution with different initial concentrations of 50−500 mg P L^{-1}. The Langmuir, Freundlich, and Temkin isotherm models were used to fit the experimental data. All the adsorption results are the average of three repetitions.

2.4. Characterization. The morphologies were observed on a scanning electron microscope coupled with an energy-dispersive spectrometer. The morphologies and pore structure of the as-prepared adsorbent were observed by transmission electron microscopy (TEM) with a Tecnai F20 transmission electron microscope (200 kV). The composition and structure of the samples were gained by powder X-ray diffraction (XRD) using a PANalytical Empyrean diffractometer with Cu Kα radiation (k = 1.5406 Å). The surface properties were detected by Fourier transform infrared spectroscopy (FTIR) on a Bruker Vector 22. The porosities were evaluated by nitrogen adsorption−desorption isotherms at ASAP 2460, and the specific surfaces were analyzed by the Brunauer−Emmitt−Teller (BET) method. X-ray photoelectron spectroscopy (XPS) spectra were collected using a Thermo Scientific ESCALAB Xi+ using Al Kα as the excitation source. The thermogravimetric analysis (TGA) tests were conducted using PerkinElmer TGA 4000 equipment from 30 to 800 °C with a heating rate of 10°/min under the air environment. The adsorption of phosphate was measured by a UV−vis spectrophotometer (HITACHI U-3900).

https://doi.org/10.1021/acsomega.4c03501
ACS Omega 2024, 9, 30826−30833

3. RESULTS AND DISCUSSION

3.1. Materials Characterization. The porous La-based adsorbents can be synthesized through a simple amination and in situ decoration process (Figure 1a). As shown in the field emission scanning electron microscopy (FESEM) image, the $La(OH)_3$/CK-DETA composite in a well-retained nanorod morphology is fabricated. The uniform $La(OH)_3$/CK-DETA composite is composed of one-dimensional (1D) strips around 1−2 μm in length and 100−200 nm in width (Figure 1b). In contrast, pure CK possesses irregular nanorods with a rough surface, whereas pure $La(OH)_3$ shows lumpy agglomeration at varied sizes due to excessive aggregation (Figure S1). No agglomeration of $La(OH)_3$ bulks is observed due to phase separation in the post decoration procedure, indicating that all $La(OH)_3$ can be well incorporated within the CK nanorods. The refinement in smooth and uniform architecture can be ameliorated by enhancing the degree of amination, as evidenced by the morphology transformation from random agglomeration to 1D smooth nanorods with the increase of DETA content (Figure S2). After a simple ultrasonic treatment, the TEM image shows a size of 1−2 μm length for the porous La-based nanorods (Figure 1c,d). Close inspection further reveals the visualized open mesopores with a size of around 26.5 nm, indicative of the porous structure (Figure 1e). The high-resolution TEM (HRTEM) image demonstrates that the porous frameworks are composed of well crystallized $La(OH)_3$ nanoparticles with a d-spacing of 0.33 nm, corresponding to the (110) plane of the hexagonal phase (Figure 1f).

The wide-angle X-ray diffraction (WAXRD) patterns (Figure 1g) display well-defined diffraction peaks at 15.6, 27.7, 39.4, 48.4, and 55.2°, which can be indexed to the 100, 110, 021, 211, and 112 reflections of the hexagonal phase, respectively, confirming the formation of the pure hexagonal phase with good crystallinity. From nitrogen sorption experiments (Figure 1h), both the $La(OH)_3$/CK-DETA composite and pure $La(OH)_3$ exhibit type IV isotherms at a high relative pressure P/P_0 = 0.8 to 1.0, indicating their uniform mesoporous structures, as also confirmed by the corresponding pore size distribution curves centered at 29.8 nm (Figure S3). The BET surface area and pore volume of the $La(OH)_3$/CK-DETA composite are calculated to be 45 $m^2\ g^{-1}$ and 0.42 $cm^3\ g^{-1}$ (Table S1), respectively. Such a good mesoporosity is capable of exposing more active sites and favoring effective transportation and contact with phosphate. The thermogravimetry (TG) curve of the La-based adsorbents exhibits a weight loss of 3.5% at around 200 °C, assigned to adsorbed water,[43] and a weight loss of 41.3% at 750 °C (Figure 1i), suggesting that the weight of residual carbon rooted in carbonized CK is about 37.8%.[44] Besides, the FTIR measurements were employed for further detection (Figure S4). The characteristic peak at 3440 cm^{-1} of pure CK, assigned to the stretching vibration of −OH, indicates the existence of massive hydroxyl groups post amination. After functionalized by DETA, the $La(OH)_3$/CK-DETA composite show additional peaks at 1640 and 1448 cm^{-1}, which can be assigned to the stretching vibration of N−H bonds[45] and the symmetric vibration of NH_2, indicative of successful amination.

3.2. Adsorption Performances. *3.2.1. Adsorption Isotherms.* The adsorption isotherm is the relationship between the initial concentration and adsorption amount when the whole adsorption reaction has reached an equilibrium state. For the adsorption isotherm experiments, a set of phosphate concentrations from 50 to 500 mg of P/L were prepared. Three different isotherm models, Langmuir, Freundlich, and Temkin, were used (Figure 2a,b and Table S2). The Langmuir model had the best fit (R^2 = 0.99) compared to the Freundlich and Temkin models, which suggests that the adsorption of the $La(OH)_3$/CK-DETA adsorbent is in the form of monomolecular layer adsorption. In the fitting curve, the adsorption amount first increases sharply and then tends to be stabilized with the gradual increase of the initial concentration. The maximum adsorption amount of phosphate by $La(OH)_3$/CK-DETA reaches 173.3 mg P g^{-1}, much higher than 127.5 mg P g^{-1} of $La(OH)_3$/CK, 107.3 mg P g^{-1} of pure $La(OH)_3$, 85.4 mg P g^{-1} of commercial $La(OH)_3$, and 45.8 mg P g^{-1} of CK-DETA (Figure 2c). The high adsorption capacity is attributed to its porous structure, high surface area, and numerous amino groups, which enables synergistic adsorption of phosphate physically and chemically. In addition, the adsorption capacity of phosphate by the synthesized $La(OH)_3$/CK-DETA is also superior among most of the reported adsorbents (Figure 2d and Table S3), demonstrating its potential as a promising alternative for phosphate removal from eutrophic water.

3.2.2. Adsorption Kinetics. Adsorption kinetics is one of the important factors in evaluating adsorption behavior. In this scenario, the effect of contact time on phosphate adsorption by $La(OH)_3$/CK-DETA, $La(OH)_3$, and CK-DETA samples was investigated in order to underline the adsorption kinetics. To obtain the adsorption kinetic parameters of each adsorbent, 0.1 g of each adsorbent was added to 0.1 L of a phosphate solution for adsorption experiments. After 30 min, the $La(OH)_3$/CK-DETA composite displays a faster adsorption rate, mainly attributed to the tremendous adsorption active sites on the surface as well as sufficient amino groups for both chemisorption and physisorption (Figure 2e). However, with the increase of adsorption time, the available adsorption active sites and amino groups gradually decrease, and the adsorption is dominated by intraparticle diffusion, which leads to gradual alleviation of the adsorption rate. The adsorption equilibrium is finally reached after 50 min, which is extremely fast. In contrast, the adsorption equilibrium of pure $La(OH)_3$ is reached after 150 min, possibly due to the single chemisorption and undesired transportation in the agglomerated structure.

These adsorption behaviors were further investigated using pseudo-first-order and pseudo-second-order models (Figure 2f and Table S4). The pseudo-second-order kinetic model better reflects the experimental data with a high correlation coefficient (R^2 = 0.99), suggesting that the main mode of adsorption for phosphate by $La(OH)_3$/CK-DETA is chemisorption. Besides, the intraparticle diffusion model also fits the kinetic data (Figure 2g), which can be divided into three stages. The first stage has a high slope and exhibits a fast surface adsorption process in which surface diffusion is the rate-limiting step. The second stage involves a slow adsorption process, mainly controlled by intraparticle diffusion before the final adsorption equilibrium in the third stage. Furthermore, the effect of the adsorbent dosage on the removal rate was also explored. The $La(OH)_3$/CK-DETA adsorbent exhibits a high removal rate of 99.8% of phosphate at a solid−liquid ratio of 1(Figure 2h), while $La(OH)_3$/CK, pure $La(OH)_3$, commercial $La(OH)_3$, and CK-DETA can remove only 75.8, 72.5, 56.8, and 45% of phosphate, respectively.

https://doi.org/10.1021/acsomega.4c03501
ACS Omega 2024, 9, 30826−30833

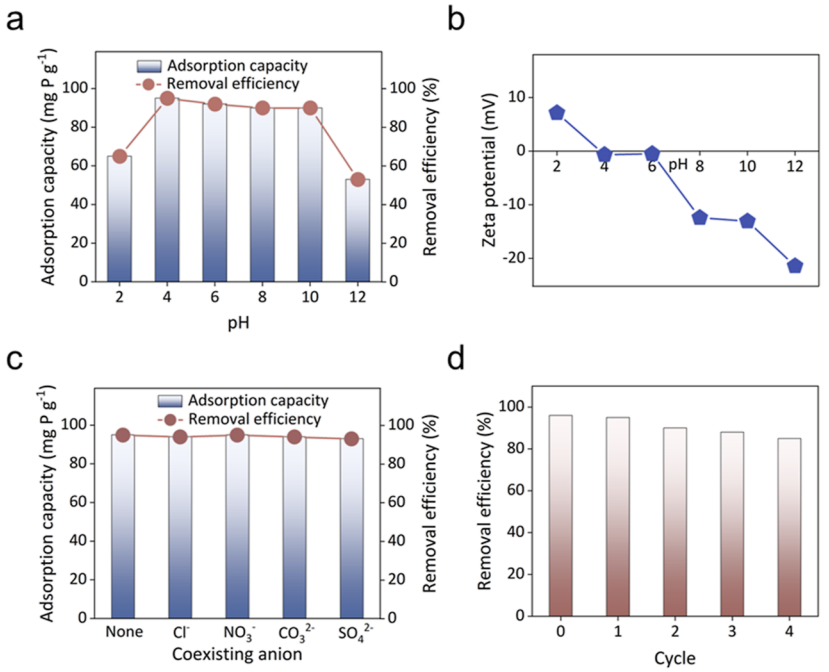

Figure 3. (a) Effects of the initial pH value on the adsorption capacity for the $La(OH)_3$/CK-DETA composite. (b) Zeta potentials of the $La(OH)_3$/CK-DETA adsorbent at varied pH values. (c) Effects of coexisting anions on phosphate adsorption. (d) Recycling of the $La(OH)_3$/CK-DETA adsorbent.

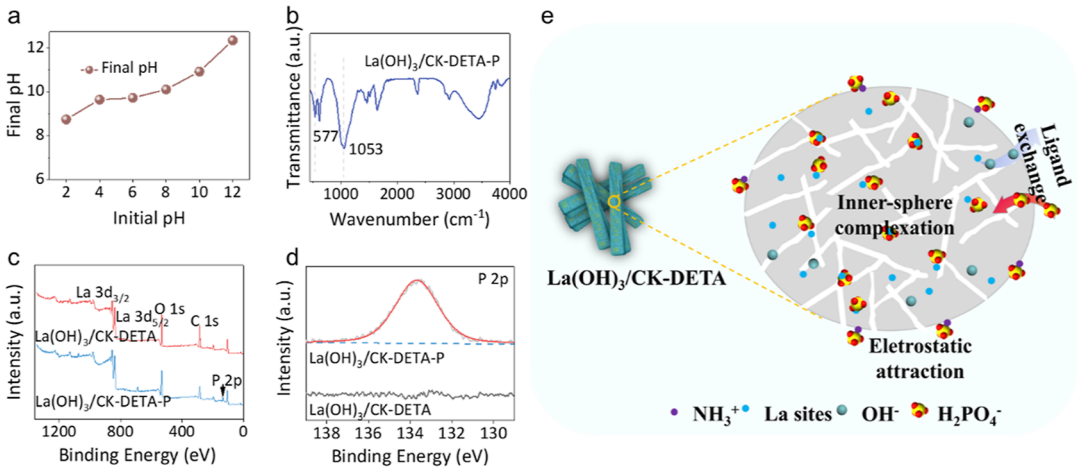

Figure 4. (a) Relationship between final and initial pH values of the solution after adsorption. (b) FTIR spectrum of the $La(OH)_3$/CK-DETA composite after adsorption. (c,d) Full-scale and high-resolution XPS spectra before and after phosphate adsorption of the $La(OH)_3$/CK-DETA adsorbent. (e) Schematic illustration of the adsorption mechanism for phosphorus removal in the $La(OH)_3$/CK-DETA composite.

3.2.3. Effect of pH, Interference Anions, and Reusability. In wastewater adsorption, pH also plays a crucial role in the electrostatic interaction between adsorbents and adsorbates; thus, phosphorus adsorption performances of $La(OH)_3$/CK-DETA at varied pH values in simulated wastewater were characterized. Typically, the phosphorus adsorption and removal rate of $La(OH)_3$/CK-DETA change considerably as the initial pH increases from 2 to 12 (Figure 3a). Under a strong acidic condition, the dissolution phenomenon occurs in the $La(OH)_3$ component, which leads to the depletion of La and consequently reduces the phosphorus adsorption. When pH > 3, $La(OH)_3$ is almost insoluble, and since the solution pH is lower than the adsorbent pH_{PZC}, the adsorbent is easy to be protonated and positively charged, favoring strong electrostatic attraction to negatively charged HPO_4^{2-} and $H_2PO_4^-$ in wastewater. Hence, the highest phosphate adsorption can be obtained at pH = 4, at which a zero-point charge value is reached (Figure 3b), and the phosphorus removal rate can reach 95%. With the increase of the pH value (pH > 4), the decline of positive charges on the adsorbent surface results in reduction of the electrostatic attraction to phosphate, leading to a gradual decrease of phosphorus adsorption. When the pH is close to 12, the presence of OH^- in solution can inhibit the ligand exchange reaction, further negatively affecting adsorption performance. These results indicate the significance of pH in adsorption of the $La(OH)_3$/CK-DETA composite. A suitable pH value that allows for both facilitating electrostatic interaction and retaining the stable adsorbent is necessary for realizing optimal adsorption performance.

https://doi.org/10.1021/acsomega.4c03501
ACS Omega 2024, 9, 30826−30833

In terms of further demonstrating the adsorbent selectivity to phosphate, phosphate removal experiments were carried out in simulated industrial and domestic wastewater containing a series of harmful anions (0.5 M CO_3^{2-}, NO_3^-, Cl^-, and SO_4^{2-}). The intrinsic removal rate of phosphate can be 96% without the addition of any coexisting anions. With the presence of coexisting anions, the phosphate removal of the $La(OH)_3$/CK-DETA adsorbent also remains over 95%, which is comparable to the intrinsic rate with no coexisting anions (Figure 3c), demonstrating the excellent selectivity to phosphate. The unaffected phosphate adsorption can be attributed to the unique affinity of lanthanum hydroxide to phosphates. Moreover, the reusability of this adsorbent was measured by conducting the phosphorus adsorption process for 5 cycles after desorption with 0.5 M NaOH. As shown in Figure 3d, the phosphate removal rate of the $La(OH)_3$/CK-DETA adsorbent is as high as 96% after the first regeneration, showing a negligible decrease. After four regeneration cycles, the phosphate removal by $La(OH)_3$/CK-DETA can be maintained at 85%, indicating good cycling stability. The slightly decreased activity is mainly due to the unavoidable precipitation of lanthanum metal during desorption,[44] as well as the partial occupation of adsorption sites from incomplete removal of phosphate during desorption.

3.3. Adsorption Mechanism Analysis. As mentioned above, the presence of abundant positively charged amino groups in the adsorbent provides strong electrostatic interaction with negatively charged phosphate ions, which plays an indispensable role in promoting the adsorption capacity of the $La(OH)_3$/CK-DETA composite. The pH_{pzc} of $La(OH)_3$/CK-DETA at 4.0 confirms that the adsorbent can be easily protonated and positively charged (Figure 3b). Alternatively, the deprotonation effect of M−OH is enhanced at pH = 12, leading to undesired electrostatic repulsion between M−O^- and the phosphate anion. In addition, other interactions apart from electrostatic force were also investigated. The pH of the simulated wastewater gradually increased after adsorption, indicating that a large amount of OH^- was generated during phosphate adsorption (Figure 4a), which is the main feature of the ligand exchange reaction. When the catalyst is added to the phosphate solution, the hydroxyl groups on the metal oxide/hydroxide adsorbent are exchanged with phosphate anions in solution and chemically immobilized on the adsorbent. During this process, the massive amount of OH^- exchanged into solution results in an increase of the pH value. It is inferred that the ligand exchange between hydroxyl and phosphate on the $La(OH)_3$/CK-DETA adsorbent plays a considerable role in phosphate adsorption. The partial contribution is derived from lanthanum phosphate generated by ligand exchange and deposited on the adsorbent surface.

We further performed SEM characterization of the product after phosphate adsorption. It is founded that a large number of white dots appeared, while the elements La, O, C, and P are uniformly distributed, indicating the successful adsorption of phosphate (Figure S5).[46,47] FTIR analysis also shows the characteristic peak at 1053 cm^{-1}, assigned to the bending vibration of P−O bond,[48] and the peak at 577 cm^{-1} related to the vibration of the La−O−P bond[49] for the $La(OH)_3$/CK-DETA-P sample after phosphate adsorption (Figure 4b). The full-spectrum XPS analysis indicates an obvious P 2p peak at 133.5 eV after adsorption of phosphate (Figure 4c,d), confirming the occurrence of phosphate adsorption. Besides, a slight shift to higher binding energies for La $3d_{3/2}$ and $3d_{5/2}$ after phosphate adsorption can be ascribed to the electron transfer during the formation of the valence band and La−O−P inner-sphere complexes (Figure S6a), implying that the inner-sphere complexes partially contribute to the phosphate adsorption, which is corroborated with the FTIR results. Meanwhile, the O 1s spectrum displays three overlapping peaks at 529.8, 531.5, and 533.1 eV, corresponding to the peaks of O^{2-}(M−O), −OH, and H_2O, respectively (Figure S6b). It is obvious to note a decrease of −OH groups and H_2O, along with an increase of O^{2-} after adsorption. This phenomenon validates the formation of the complex La−O−P during phosphate adsorption.

Based on the above observations, the excellent adsorption performance to phosphate can be attributed to the combination of both chemisorption and physisorption of the designed $La(OH)_3$/CK-DETA composite. The contribution of phosphate adsorption consists of electrostatic attraction, inner-sphere complexation, and ligand exchange (Figure 4e). First, the amination with DETA affords the introduction of plenty of amino groups, which could transform to positively charged NH^{3+} by protonation to adsorb $H_2PO_4^-$ or HPO_4^{2-} through electrostatic attraction. At the same time, by inner-sphere complexation and ligand exchange of lanthanum, certain lanthanum phosphate precipitates can be generated and attached to the interior cavity of the high-surface-area adsorbent. Such a uniform porous nanostructure for exposure of active sites, in combination with abundant functionalized amino groups for advantageous chemisorption, contributes to the superior adsorption capacity, selectivity, and cyclability of the designed $La(OH)_3$/CK-DETA composite adsorbent.

4. CONCLUSIONS

In summary, an environmentally friendly, low-cost, and highly efficient $La(OH)_3$/CK-DETA adsorbent was prepared by a simple functionalization and in situ growth method. The $La(OH)_3$ was homogeneously anchored in nanorods, which increased its dispersibility and facilitated the adsorption of phosphate with its high specific surface area and large pore size. The maximum adsorption capacity of the $La(OH)_3$/CK-DETA adsorbent was 173.3 mg P g^{-1}, much higher than that of most of the reported adsorbents. Also, the adsorption equilibrium could be reached within 50 min, showing the ultrafast adsorption of phosphate. In addition, in the presence of 0.5 M anions (CO_3^{2-}, NO_3^-, Cl^-, and SO_4^{2-}), the composite adsorbent showed excellent selectivity and immunity to phosphate. Mechanistic studies showed that electrostatic attraction, inner-sphere complexation, and ligand exchange reactions together contributed to excellent phosphate adsorption behavior. Our study provides a comprehensive design solution for realizing high-performance adsorbents for wastewater treatment.

■ ASSOCIATED CONTENT

Supporting Information

The Supporting Information is available free of charge at https://pubs.acs.org/doi/10.1021/acsomega.4c03501.

Analysis of the complexes through SEM, N_2 adsorption isotherms, infrared spectroscopy, and XPS and tables summarizing the physical properties of all materials, adsorption parameters, and comparison of adsorption with that of other adsorbents (PDF)

https://doi.org/10.1021/acsomega.4c03501
ACS Omega 2024, 9, 30826−30833

AUTHOR INFORMATION

Corresponding Authors

Mei Xue − *College of Energy Materials and Chemistry, College of Chemistry and Chemical Engineering, Inner Mongolia Engineering and Technology Research Center for Catalytic Conversion and Utilization of Carbon Resource Molecules, Inner Mongolia University, Hohhot 010021, P. R. China*; Email: setsubai@sina.cn

Kun Lan − *College of Energy Materials and Chemistry, College of Chemistry and Chemical Engineering, Inner Mongolia Engineering and Technology Research Center for Catalytic Conversion and Utilization of Carbon Resource Molecules, Inner Mongolia University, Hohhot 010021, P. R. China*; orcid.org/0000-0001-8983-0155; Email: k_lan@imu.edu.cn

Authors

Yalin He − *College of Energy Materials and Chemistry, College of Chemistry and Chemical Engineering, Inner Mongolia Engineering and Technology Research Center for Catalytic Conversion and Utilization of Carbon Resource Molecules, Inner Mongolia University, Hohhot 010021, P. R. China*

Xingyue Qi − *College of Energy Materials and Chemistry, College of Chemistry and Chemical Engineering, Inner Mongolia Engineering and Technology Research Center for Catalytic Conversion and Utilization of Carbon Resource Molecules, Inner Mongolia University, Hohhot 010021, P. R. China*

Jialong Li − *College of Energy Materials and Chemistry, College of Chemistry and Chemical Engineering, Inner Mongolia Engineering and Technology Research Center for Catalytic Conversion and Utilization of Carbon Resource Molecules, Inner Mongolia University, Hohhot 010021, P. R. China*

Wendi Wang − *College of Energy Materials and Chemistry, College of Chemistry and Chemical Engineering, Inner Mongolia Engineering and Technology Research Center for Catalytic Conversion and Utilization of Carbon Resource Molecules, Inner Mongolia University, Hohhot 010021, P. R. China*

Jingyu Zhang − *College of Energy Materials and Chemistry, College of Chemistry and Chemical Engineering, Inner Mongolia Engineering and Technology Research Center for Catalytic Conversion and Utilization of Carbon Resource Molecules, Inner Mongolia University, Hohhot 010021, P. R. China*

Lanhao Yang − *College of Energy Materials and Chemistry, College of Chemistry and Chemical Engineering, Inner Mongolia Engineering and Technology Research Center for Catalytic Conversion and Utilization of Carbon Resource Molecules, Inner Mongolia University, Hohhot 010021, P. R. China*

Complete contact information is available at: https://pubs.acs.org/10.1021/acsomega.4c03501

Notes

The authors declare no competing financial interest.

ACKNOWLEDGMENTS

This work was supported by the National Natural Science Foundation of China (22205118 and 22375108), "Junma" Program of Inner Mongolia University, Grassland Talent Program of Inner Mongolia, Young Talents of Science and Technology of Inner Mongolia (NJYT23037), and Natural Science Foundation of Inner Mongolia (2023JQ06).

REFERENCES

(1) Xie, S.; Wu, S.; Bao, S.; Wang, Y.; Zheng, Y.; Deng, D.; Huang, L.; Zhang, L.; Lee, M.; Huang, Z. Intelligent Mesoporous Materials for Selective Adsorption and Mechanical Release of Organic Pollutants from Water. *Adv. Mater.* **2018**, *30* (27), 1800683.

(2) Lin, B.; Wang, A.; Guo, Y.; Ding, Y.; Zhan, W.; Wang, L.; Guo, Y.; Gao, F. Elimination of NO pollutant in semi-enclosed spaces over sodium-promoted cobalt oxyhydroxide (CoOOH) by oxidation and adsorption mechanism. *Appl. Catal., B* **2020**, *279*, 119404.

(3) Zhu, C.; Lu, L.; Fang, Q.; Song, S.; Chen, B.; Shen, Y. Unveiling Spin State-Dependent Micropollutant Removal using Single-Atom Covalent Triazine Framework. *Adv. Funct. Mater.* **2023**, *33* (19), 2210905.

(4) Xie, L.; Wang, P.; Li, Y.; Zhang, D.; Shang, D.; Zheng, W.; Xia, Y.; Zhan, S.; Hu, W. Pauling-type adsorption of O2 induced electrocatalytic singlet oxygen production on N-CuO for organic pollutants degradation. *Nat. Commun.* **2022**, *13* (1), 5560.

(5) Huang, D.; Wu, J.; Wang, L.; Liu, X.; Meng, J.; Tang, X.; Tang, C.; Xu, J. Novel insight into adsorption and co-adsorption of heavy metal ions and an organic pollutant by magnetic graphene nanomaterials in water. *Chem. Eng. J.* **2019**, *358*, 1399−1409.

(6) Peydayesh, M.; Suter, M. K.; Bolisetty, S.; Boulos, S.; Handschin, S.; Nyström, L.; Mezzenga, R. Amyloid Fibrils Aerogel for Sustainable Removal of Organic Contaminants from Water. *Adv. Mater.* **2020**, *32* (12), 1907932.

(7) Wang, F.; Gao, Y.; Fu, H.; Liu, S.-S.; Wei, Y.; Wang, P.; Zhao, C.; Wang, J.-F.; Wang, C.-C. Almost 100% electron transfer regime over Fe-Co dual-atom catalyst toward pollutants removal: Regulation of peroxymonosulfate adsorption mode. *Appl. Catal., B* **2023**, *339*, 123178.

(8) Ng, S. W. L.; Yilmaz, G.; Ong, W. L.; Ho, G. W. One-step activation towards spontaneous etching of hollow and hierarchical porous carbon nanospheres for enhanced pollutant adsorption and energy storage. *Appl. Catal., B* **2018**, *220*, 533−541.

(9) Huang, H.; Zhang, P.; Zhang, Z.; Liu, J.; Xiao, J.; Gao, F. Simultaneous removal of ammonia nitrogen and recovery of phosphate from swine wastewater by struvite electrochemical precipitation and recycling technology. *J. Cleaner Prod.* **2016**, *127*, 302−310.

(10) Idris, A.; Hassan, N.; Mohd Ismail, N. S.; Misran, E.; Yusof, N. M.; Ngomsik, A.-F.; Bee, A. Photocatalytic magnetic separable beads for chromium (VI) reduction. *Water Res.* **2010**, *44* (6), 1683−1688.

(11) He, J.; Wang, W.; Sun, F.; Shi, W.; Qi, D.; Wang, K.; Shi, R.; Cui, F.; Wang, C.; Chen, X. Highly Efficient Phosphate Scavenger Based on Well-Dispersed La(OH)3 Nanorods in Polyacrylonitrile Nanofibers for Nutrient-Starvation Antibacteria. *ACS Nano* **2015**, *9* (9), 9292−9302.

(12) Withers, P. J. A.; Elser, J. J.; Hilton, J.; Ohtake, H.; Schipper, W. J.; van Dijk, K. C. Greening the global phosphorus cycle: how green chemistry can help achieve planetary P sustainability. *Green Chem.* **2015**, *17* (4), 2087−2099.

(13) Chen, M.; Liu, T.; Zhang, X.; Zhang, R.; Tang, S.; Yuan, Y.; Xie, Z.; Liu, Y.; Wang, H.; Fedorovich, K. V.; et al. Photoinduced Enhancement of Uranium Extraction from Seawater by MOF/Black Phosphorus Quantum Dots Heterojunction Anchored on Cellulose Nanofiber Aerogel. *Adv. Funct. Mater.* **2021**, *31* (22), 2100106.

(14) Mayer, B. K.; Baker, L. A.; Boyer, T. H.; Drechsel, P.; Gifford, M.; Hanjra, M. A.; Parameswaran, P.; Stoltzfus, J.; Westerhoff, P.; Rittmann, B. E. Total Value of Phosphorus Recovery. *Environ. Sci. Technol.* **2016**, *50* (13), 6606−6620.

(15) Kabay, N.; Arar, O.··; Samatya, S.; Yüksel, Ü.; Yüksel, M. Separation of fluoride from aqueous solution by electrodialysis: Effect of process parameters and other ionic species. *J. Hazard. Mater.* **2008**, *153* (1−2), 107−113.

(16) Wang, L.; Wen, X.; Li, J.; Zeng, P.; Song, Y.; Yu, H. Roles of defects and linker exchange in phosphate adsorption on UiO-66 type metal organic frameworks: Influence of phosphate concentration. *Chem. Eng. J.* **2021**, *405*, 126681.
(17) Lan, Z.; Lin, Y.; Yang, C. Lanthanum-iron incorporated chitosan beads for adsorption of phosphate and cadmium from aqueous solutions. *Chem. Eng. J.* **2022**, *448*, 137519.
(18) Lu, S. G.; Bai, S. Q.; Zhu, L.; Shan, H. D. Removal mechanism of phosphate from aqueous solution by fly ash. *J. Hazard. Mater.* **2009**, *161* (1), 95−101.
(19) Xie, J.; Wang, Z.; Lu, S.; Wu, D.; Zhang, Z.; Kong, H. Removal and recovery of phosphate from water by lanthanum hydroxide materials. *Chem. Eng. J.* **2014**, *254*, 163−170.
(20) Zhao, S.; Malfait, W. J.; Guerrero-Alburquerque, N.; Koebel, M. M.; Nyström, G. Biopolymer Aerogels and Foams: Chemistry, Properties, and Applications. *Angew. Chem., Int. Ed.* **2018**, *57* (26), 7580−7608.
(21) Kou, D.; Ma, W.; Zhang, S. Functionalized Mesoporous Photonic Crystal Film for Ultrasensitive Visual Detection and Effective Removal of Mercury (II) Ions in Water. *Adv. Funct. Mater.* **2021**, *31* (9), 2007032.
(22) Zhang, X.; Shen, J.; Pan, S.; Qian, J.; Pan, B. Metastable Zirconium Phosphate under Nanoconfinement with Superior Adsorption Capability for Water Treatment. *Adv. Funct. Mater.* **2020**, *30* (12), 1909014.
(23) Liu, R.; Chi, L.; Wang, X.; Wang, Y.; Sui, Y.; Xie, T.; Arandiyan, H. Effective and selective adsorption of phosphate from aqueous solution via trivalent-metals-based amino-MIL-101 MOFs. *Chem. Eng. J.* **2019**, *357*, 159−168.
(24) Ahmadijokani, F.; Molavi, H.; Rezakazemi, M.; Tajahmadi, S.; Bahi, A.; Ko, F.; Aminabhavi, T. M.; Li, J.-R.; Arjmand, M. UiO-66 metal-organic frameworks in water treatment: A critical review. *Prog. Mater. Sci.* **2022**, *125*, 100904.
(25) Feng, L.; Zhang, Q.; Ji, F.; Jiang, L.; Liu, C.; Shen, Q.; Liu, Q. Phosphate removal performances of layered double hydroxides (LDH) embedded polyvinyl alcohol/lanthanum alginate hydrogels. *Chem. Eng. J.* **2022**, *430*, 132754.
(26) Keyikoglu, R.; Khataee, A.; Yoon, Y. Layered double hydroxides for removing and recovering phosphate: Recent advances and future directions. *Adv. Colloid Interface Sci.* **2022**, *300*, 102598.
(27) Ikhlaq, A.; Brown, D. R.; Kasprzyk-Hordern, B. Catalytic ozonation for the removal of organic contaminants in water on ZSM-5 zeolites. *Appl. Catal., B* **2014**, *154*−*155*, 110−122.
(28) Rehman, S.; Guo, S.; Hou, Y. Porous Carbon Spheres: Rational Design of Si/SiO2@Hierarchical Porous Carbon Spheres as Efficient Polysulfide Reservoirs for High-Performance Li-S Battery (Adv. Mater. 16/2016). *Adv. Mater.* **2016**, *28* (16), 3166.
(29) Zheng, J.; Wahiduzzaman, M.; Barpaga, D.; Trump, B. A.; Gutiérrez, O. Y.; Thallapally, P.; Ma, S.; McGrail, B. P.; Maurin, G.; Motkuri, R. K. Porous Covalent Organic Polymers for Efficient Fluorocarbon-Based Adsorption Cooling. *Angew. Chem., Int. Ed.* **2021**, *60* (33), 18037−18043.
(30) Li, S.; Huang, X.; Wan, Z.; Liu, J.; Lu, L.; Peng, K.; Schmidt-Ott, A.; Bhattarai, R. Green synthesis of ultrapure La(OH)3 nanoparticles by one-step method through spark ablation and electrospinning and its application to phosphate removal. *Chem. Eng. J.* **2020**, *388*, 124373.
(31) Wang, Z.; Xia, D.; Cui, S.; Yu, W.; Wang, B.; Liu, H. A high-capacity nanocellulose aerogel uniformly immobilized with a high loading of nano-La(OH)3 for phosphate removal. *Chem. Eng. J.* **2022**, *433*, 134439.
(32) Liao, T.; Li, T.; Su, X.; Yu, X.; Song, H.; Zhu, Y.; Zhang, Y. La(OH)3-modified magnetic pineapple biochar as novel adsorbents for efficient phosphate removal. *Bioresour. Technol.* **2018**, *263*, 207−213.
(33) Yu, J.; Xiang, C.; Zhang, G.; Wang, H.; Ji, Q.; Qu, J. Activation of Lattice Oxygen in LaFe (Oxy)hydroxides for Efficient Phosphorus Removal. *Environ. Sci. Technol.* **2019**, *53* (15), 9073−9080.
(34) Dong, S.; Wang, Y.; Zhao, Y.; Zhou, X.; Zheng, H. La3+/La(OH)3 loaded magnetic cationic hydrogel composites for phosphate removal: Effect of lanthanum species and mechanistic study. *Water Res.* **2017**, *126*, 433−441.
(35) Zong, E.; Huang, G.; Liu, X.; Lei, W.; Jiang, S.; Ma, Z.; Wang, J.; Song, P. A lignin-based nano-adsorbent for superfast and highly selective removal of phosphate. *J. Mater. Chem. A* **2018**, *6* (21), 9971−9983.
(36) Bai, J.; Huang, Y.; Gong, Q.; Liu, X.; Li, Y.; Gan, J.; Zhao, M.; Shao, Y.; Zhuang, D.; Liang, J. Preparation of porous carbon nanotube/carbon composite spheres and their adsorption properties. *Carbon* **2018**, *137*, 493−501.
(37) Zhang, L.; Zhou, Q.; Liu, J.; Chang, N.; Wan, L.; Chen, J. Phosphate adsorption on lanthanum hydroxide-doped activated carbon fiber. *Chem. Eng. J.* **2012**, *185*−*186*, 160−167.
(38) Wang, Z.; Wang, H.; Li, Q.; Xu, M.; Guo, Y.; Li, J.; Wu, T. pH effect on Re(VII) and Se(IV) diffusion in compacted GMZ bentonite. *Appl. Geochem.* **2016**, *73*, 1−7.
(39) Jia, X.; Wang, H.; Li, Y.; Xu, J.; Cheng, H.; Li, M.; Zhang, S.; Zhang, H.; Hu, G. Separable lanthanum-based porous PAN nanofiber membrane for effective aqueous phosphate removal. *Chem. Eng. J.* **2022**, *433*, 133538.
(40) Feng, W.; Wang, T.; Zhu, Y.; Sun, F.; Giesy, J. P.; Wu, F. Chemical composition, sources, and ecological effect of organic phosphorus in water ecosystems: a review. *Carbon Res.* **2023**, *2* (1), 12.
(41) Fang, L.; Shi, Q.; Nguyen, J.; Wu, B.; Wang, Z.; Lo, I. M. C. Removal Mechanisms of Phosphate by Lanthanum Hydroxide Nanorods: Investigations using EXAFS, ATR-FTIR, DFT, and Surface Complexation Modeling Approaches. *Environ. Sci. Technol.* **2017**, *51* (21), 12377−12384.
(42) Jia, X.; Zhao, X.; Bi, Z.; Zhang, H.; Huang, S.; Chun-Ho Lam, J.; Li, W.; Li, Y.; Wågberg, T.; Hu, G. Rod-shaped lanthanum oxychloride-decorated porous carbon material for efficient and ultra-fast removal of phosphorus from eutrophic water. *Sep. Purif. Technol.* **2023**, *306*, 122713.
(43) Guan, T.; Li, X.; Fang, W.; Wu, D. Efficient removal of phosphate from acidified urine using UiO-66 metal-organic frameworks with varying functional groups. *Appl. Surf. Sci.* **2020**, *501*, 144074.
(44) Al-Wabel, M. I.; Al-Omran, A.; El-Naggar, A. H.; Nadeem, M.; Usman, A. R. A. Pyrolysis temperature induced changes in characteristics and chemical composition of biochar produced from conocarpus wastes. *Bioresour. Technol.* **2013**, *131*, 374−379.
(45) Cavani, F.; Trifirò, F.; Vaccari, A. Hydrotalcite-type anionic clays: Preparation, properties and applications. *Catal. Today* **1991**, *11* (2), 173−301.
(46) Jia, X.; Zhao, X.; Zhou, Y.; Li, F.; Liu, W.; Huang, Y.; Zhang, H.; Ma, J.; Hu, G. Tri-functional lanthanum-based biochar for efficient phosphorus recovery, bacterial inhibition, and soil fertility enhancement. *Biochar* **2023**, *5* (1), 16.
(47) Jia, X.; Yin, T.; Wang, Y.; Zhou, S.; Zhao, X.; Chen, W.; Hu, G. Porous honeycomb cork biochar for efficient and highly selective removal of phosphorus from wastewater. *Biochar* **2023**, *5* (1), 84.
(48) Lucas, I. T.; McLeod, A. S.; Syzdek, J. S.; Middlemiss, D. S.; Grey, C. P.; Basov, D. N.; Kostecki, R. IR Near-Field Spectroscopy and Imaging of Single Li_xFePO_4 Microcrystals. *Nano Lett.* **2015**, *15* (1), 1−7.
(49) Ghosh, P.; Oliva, J.; Rosa, E. D. l.; Haldar, K. K.; Solis, D.; Patra, A. Enhancement of Upconversion Emission of LaPO4:Er@Yb Core-Shell Nanoparticles/Nanorods. *J. Phys. Chem. C* **2008**, *112* (26), 9650−9658.

https://doi.org/10.1021/acsomega.4c03501
ACS Omega 2024, 9, 30826−30833